Character of valence-band states in the Kondo surface alloys $CeAg_x$/Ag(111) and $CePt_5$/Pt(111)

H. Schwab and M. Mulazzi
Universität Würzburg, Experimentelle Physik VII, Am Hubland, D-97074 Würzburg, Germany

J. Jiang, H. Hayashi, T. Habuchi, and D. Hirayama
Graduate School of Science, Hiroshima University, Higashi-Hiroshima 739-8526, Japan

H. Iwasawa and K. Shimada
Hiroshima Synchrotron Radiation Center, Hiroshima University, Higashi-Hiroshima 739-0046, Japan

F. Reinert
Universität Würzburg, Experimentelle Physik VII, Am Hubland, D-97074 Würzburg, Germany, and
Karlsruhe Institute of Technology KIT, Gemeinschaftslabor für Nanoanalytik, D-76021 Karlsruhe, Germany

(Received 2 December 2011; revised manuscript received 13 February 2012; published 27 March 2012)

The crystal and electronic structures of the $CePt_5$ and $CeAg_x$ surface alloys have been investigated by means of low-energy electron diffraction and angle-resolved photoelectron spectroscopy. From measurements performed near the $4d$-$4f$ absorption edge we were able to infer the weight of the $4f$-electron spectral function with respect to the single-particle density of states. While the typical Kondo features at the Fermi energy (Kondo resonance and spin-orbit partner) in the $CePt_5$ surface alloy were observed, only the f^0 ionization structure and the spin-orbit partner were present in the $CeAg_x$ case. From our experiments, and by comparison to model calculations, we were able to estimate the Kondo temperature in the two systems and investigate parameters contributing to the hybridization strength.

DOI: 10.1103/PhysRevB.85.125130 PACS number(s): 75.20.Hr, 74.25.Jb, 76.30.Kg

I. INTRODUCTION

Systems of rare earths combined with transition metals are rich with interesting properties originating from the interaction of the localized $4f$ electrons of the rare earth and the more itinerant d electrons of the transition metals. The hybridization between d and f electrons gives rise to the Kondo effect at sufficiently low temperatures and at even lower temperatures to the formation of coherent quasiparticles[1] and in some cases to heavy fermion superconductivity.[2] The large majority of the studies in this field have focused on bulk crystals, while little interest has been given to artificially prepared surface alloys. Using state-of-the-art surface science techniques it is possible to completely control the cleanliness of the substrate and the growth of the surface alloy, namely, the stoichiometry and the crystal structure, and to check for the presence of spurious phases or surface reconstructions. None of this is possible when using cleaved bulk single crystals. A second motivation for the study of cerium-transition-metal surface alloys is the reduced thickness of the region of interest forming on the substrate, which leads to an effective reduction of the dimensionality. It is known that in low dimensions the physical properties of matter change drastically, mainly because of the reduced coordination.[3,4]

Resistivity measurements of bulk $CePt_5$ have shown a minimum at $T = 9$ K attributed to the Kondo effect.[5] However, at lower temperatures specific heat and magnetic susceptibility revealed antiferromagnetic order, but no indication of heavy fermion behavior was found in the three-dimensional material.[6] On the other hand, the formation of a heavy fermion band was shown in the surface alloy of $CePt_5$/Pt(111),[1] proving that the low-temperature behavior of surface $CePt_5$ and the low-temperature behavior of bulk $CePt_5$ differ considerably. Since the macroscopic properties of the alloys depend strongly on the degree of hybridization between the f electrons and the conduction bands, we investigated another compound, namely, $CeAg_x$, which has a different electron filling with respect to $CePt_5$. Unfortunately not very much is known about the magnetic properties of bulk CeAg systems. Several works dedicated to bulk CeAg (Refs. 7–9) report about ferromagnetic order at $T < 5.5$ K, while experimental studies devoted to the properties of cerium and silver surface alloys are necessary. Therefore, we investigated the properties of the two surface alloys, $CePt_5$ and $CeAg_x$, with the purpose of characterizing the high-energy excitations and the overall electronic structure.

II. BASIC THEORETICAL DESCRIPTION

A small amount of magnetic impurities diluted into a metallic host has drastic effects on the resistivity. Instead of parabolically decreasing and saturating at zero temperature, as in the case of a usual Fermi liquid, the resistivity shows a characteristic minimum in the temperature dependence and then an upturn at even lower temperatures. The effect was found in the 1930s,[10] but it was several decades before a satisfactory theoretical explanation was put forth.[11] The resistivity minimum occurs at the so-called Kondo temperature T_K which, in the framework of the single-impurity regime, is given by[12]

$$k_B T_K \sim D \exp\left(-\frac{1}{2J\rho(E_F)}\right). \quad (1)$$

Here k_B is the Boltzmann constant, D is the conduction band width, $\rho(E_F)$ is the density of conducting states at the

Fermi energy E_F, and J is the coupling constant between the magnetic impurities and the conduction electrons.[12]

While this result was obtained using the s-d model Hamiltonian, a more fundamental description of the interactions between localized and itinerant particles is given by the single-impurity Anderson model (SIAM),[13] whose building blocks are (i) the conduction band states, (ii) the energy of the localized f electron, (iii) the Coulomb repulsion energy occurring when two electrons occupy the f states, and (iv) the hybridization between f and conduction electrons. Including a possible interaction between inequivalent cerium sites, one obtains the periodic Anderson model, which is used to model the formation of heavy quasiparticles at $T < T_K$. On the basis of this Hamiltonian, the thermodynamical proprties of cerium alloys can be calculated and compared to experiments. The spectral function can also be obtained and compared to photoemission data, as they measure it directly.[14]

The ground state configuration of Kondo systems is a linear combination of the possible electronic configurations of the Ce impurity, f^0, f^1, or f^2, depending on how many electrons occupy the f shell. With no hybridization and in the limit of infinitely large Coulomb repulsion, the f state is single occupied (f^1 state) while at finite hybridization the f electron can be transferred into the conduction band, lowering the f-occupation number $n_f < 1$. For finite U, the double occupancy is allowed (f^2 state) but in general its contribution is very small, given the large value of U for typical f systems (between 5 and 10 eV).[15]

To calculate the spectral function in the framework of the SIAM,[16–20] one needs the final state configurations accessible from the ground state by an electron removal, for photoemission (PES), or addition, for inverse photoemission (IPES). As we are mostly concerned here with photoemission data, we are describing only the case of electron removal. If the occupation in the ground state is 1 (f^1 state) then the PES final state has no f electrons. This transition gives rise to an ionization peak (IS), identified as a broad structure a few electronvolts below the Fermi energy. The excitations at low energies are responsible for the Kondo effect and they involve the spin flipping of the electrons on the f site. In particular, the hybridization introduces an antiferromagnetic coupling between the f electrons and the conduction electrons, lowering the energy of the singlet with respect to the triplet state. Hence in configuration terms, the singlet is a linear combination of f^0 and f^1 states. Upon removal of one electron, the system can make a transition to an f^1 final state, provided that one electron from the conduction band fills the hole left by the photoelectron. This process originates a peak near the Fermi energy, generally named Kondo resonance (KR), which is the main interest of this paper. These transitions produce the main features of the spectral functions, while neglecting weaker interactions like spin-orbit splitting (≈280 meV) and crystal field effects(≈30 meV) which yield satellites to the KR, namely, the spin-orbit (SO) and the crystal-field satellite. They give rise to spectral features that have been observed in experiments[18,19] and can be fully taken into account in calculations.

A direct measurement of the f-only spectral function is possible by employing resonant photoemission, i.e., measuring the valence band spectrum tuning the photon energy close to a core-level absorption edge. The $4f$-derived spectral intensity shows a Fano-like resonant enhancement[21] due to the interference between a direct photoemission process, $d^{10}4\ f^1 + h\nu \rightarrow d^{10}4\ f^0 + e^-$, and a photoabsorption followed by an Auger transition, $d^{10}4\ f^1 + h\nu \rightarrow d^9 4\ f^2 \rightarrow d^{10}4\ f^0 + e^-$. This intermediate state autoionizes (Coster-Kronig transition) with one $4f$ electron falling into the core hole and the other reaching the analyzer. Resonant photoemission has two advantages: the photoelectron yield increases strongly at the resonance and the measurement is very sensitive to the intermediate state electrons. For the measurements here reported, the $4d \rightarrow 4f$ transition was chosen, which occurs at a photon energy of about 122 eV.

Measurements taken with linearly polarized light are sensitive to the symmetry of the wave functions as the latter can only be even or odd with respect to the crystal mirror plane. Since the final state (in the free electron approximation) is even, the choice of the photon polarization (parallel or perpendicular to a mirror plane) directly tells the symmetry of the initial state wave function with respect to a chosen mirror plane, which is an important aspect for angle-resolved photoelectron spectroscopy (ARPES) measurements.

In the following we discuss on- and off-resonant ARPES data of $CePt_5$ and $CeAg_x$, focusing on how the photoemission intensity can be related to the hybridization, its dependence on atomic properties and how they affect the Kondo temperature. These aspects were explored theoretically by Gunnarsson and Schönhammer,[16] while the experimental work dealt with vacuum-scraped bulk polycrystals[17] or with sub-monolayer Ce adatoms on metal surfaces.[20] Here we investigate surface alloys, which offer the advantages of giving spectra independent of the surface preparation (once optimized) and of stoichiometry independent of the evaporation rate, as it is controlled by the alloying process.

III. EXPERIMENTAL

A. ARPES measurements

The experiments were performed on the linear undulator beamline (BL-1) of a compact electron-storage ring (HiSOR) at Hiroshima Synchrotron Radiation Center in Japan. BL-1 provides photons in the energy range 22–300 eV with s- and p-polarization geometries, tunable by rotating the endstation around the synchrotron's light beam. The endstation is equipped with a VG Scienta R4000 electron analyzer and a five-axis cryostat. During this experiment the energy resolution at the resonance energy was set at $\Delta E = 50$ meV. The sample was cooled to 10 K, as measured on the manipulator cold finger, and kept at this temperature during all the ARPES data acquisition time. The degree of surface crystallinity was determined by low-energy electron diffraction (LEED) and the cleanliness with Auger electron spectroscopy (AES).

B. Preparation of surface alloys and characterization

Cerium evaporation on Pt(111) and subsequent annealing results in a surface alloy with a very rich phase diagram that was previously investigated by LEED and AES.[22] A well-ordered structure can be obtained by evaporating 2 monolayers

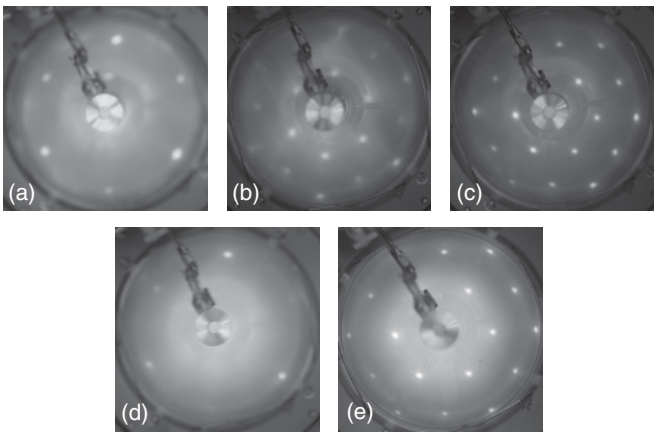

FIG. 1. LEED images of the different cerium alloys at 70 eV kinetic energy of the incident electrons: (a) 1×1 reconstruction of clean Pt(111), (b) 2×2 reconstruction of 0.5 ML $CePt_5$/Pt(111), (c) $(2 \times 2)R30^\circ$ reconstruction of 2 ML $CePt_5$/Pt(111), (d) 1×1 reconstruction of clean Ag(111), and (e) $(2 \times 2)R30^\circ$ reconstruction of 2 ML $CeAg_x$/Ag(111).

(ML) of cerium on the surface and annealing to 550 °C. This $CePt_5$ surface alloy shows a $(2 \times 2)R30^\circ$ reconstruction under LEED [see Fig. 1(c)].[22] In our experiments the evaporation rate was calibrated using the (2×2) reconstruction [Fig. 1(b)] that forms after deposition of 0.5 ML and subsequent annealing. The films investigated in this paper were four unit cells of $CePt_5$ or 18 Å thick. After evaporation of 2 ML of Ce on a heated to 4 °C Ag(111) surface we observed a $(2 \times 2)R30^\circ$ reconstruction [Fig. 1(e)], similar to the 2 ML $CePt_5$/Pt(111) surface alloy in Fig. 1(c). Since the structure of the $CeAg_x$ surface alloy is unknown we cannot state a film thickness here.

The surface contamination was monitored by means of AES (not shown). In no case was a signal in the vicinity of 530 eV indicating the lack of oxygen on the surface observed. Assuming that the oxygen intensity in the $\frac{dI}{dV}$ spectrum is as large as the noise of the signal, and comparing this intensity to the Ce after annealing, we can give 0.04 ML as an upper limit for oxygen coverage. Given that cerium easily reacts with oxygen and the latter was detected several hours after the surface preparation, we conclude that the surface is terminated by a silver capping layer that prevents oxidation. For $CePt_5$/Pt(111) the formation of a Pt capping layer was observed by CO adsorbtion measured with high-resolution electron energy loss spectroscopy.[22]

IV. PHOTOEMISSION RESULTS

A. 4f spectral function of $CeAg_x$/Ag(111)

The 4f spectral function in Fig. 2(a) shows three features: (i) the IS dominating the spectrum with a binding energy (energy below E_F) of $E_B = 2.2$ eV, (ii) the SO peak at a binding energy of $E_B = 0.27$ eV, and (iii) a very small shoulder right at the Fermi energy, where the KR is normally located. The weakness of the Kondo peak can be attributed to either a weak hybridization or to excessive experimental temperature, $T \gg T_K$. However, the higher intensity of the SO peak with respect to the true Kondo peak at the Fermi

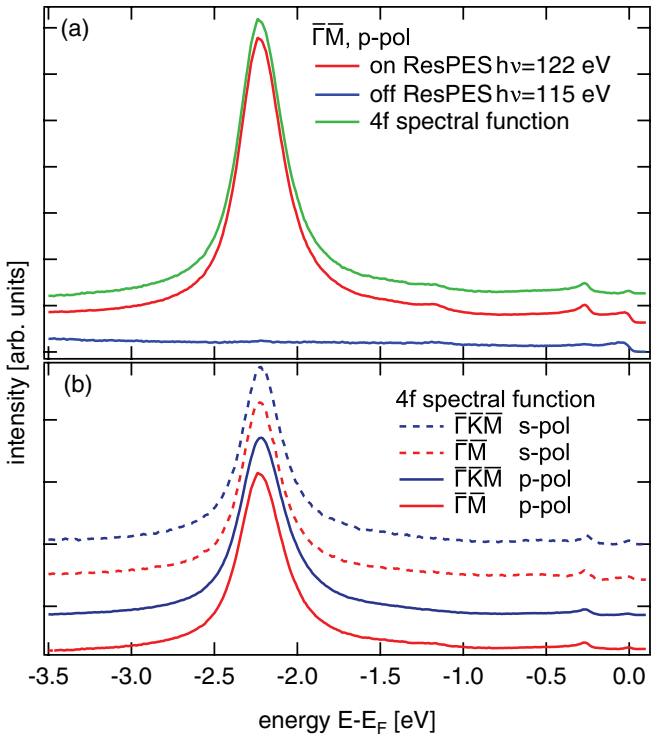

FIG. 2. (Color online) (a) Momentum integrated off-resonance (blue) and on-resonance (red) experimental ARPES data for $CeAg_x$ measured along $\bar{\Gamma}\bar{M}$ with p polarization, the green curve shows the difference between the data at on and off resonance that represent the f spectral function. (b) f spectral functions measured along different high-symmetry directions with s- and p-polarized light, as indicated in the label.

energy hints at a weak hybridization regime, as pointed out by model calculations.[17] The spectral functions measured for the other high-symmetry directions and light polarizations in Fig. 2(b) share the same features, supporting this description.

B. 4f spectral function of $CePt_5$/Pt(111)

The 4f spectral function of the $CePt_5$/Pt(111) surface alloy is shown in Fig. 3(a). It displays the occupied part of the Kondo resonance right at the Fermi energy and its SO partner as a shoulder at $E_B = 0.27$ eV. At higher binding energies several additional features appear, which we attribute to either the substrate [in clean platinum the 5d bands disperse from above the Fermi energy down to $E_B = 7.5$ eV (Ref. 23)] or the Pt atoms forming the surface alloy. The 7-eV difference between the on- and off-resonant excitation energies implies a variation of the k_z probed by the two measurements. Given the perpendicular dispersion of (at least) the substrate Pt bands, we conclude that part of the intensity observed in the f spectral function receives a contribution from the single-particle density of states of Pt. And indeed the Pt band structure along the ΓL direction shows dispersing bands from the Fermi energy down to $E_B = 5$ eV.[23] Moreover, a step in the real part of the hybridization in the energy range of the on-site energy can induce a splitting of the IS.[20] In the Pt band structure several bands have extrema at $E_B \approx 2$ eV, leading to a step in the density of states at that energy which again

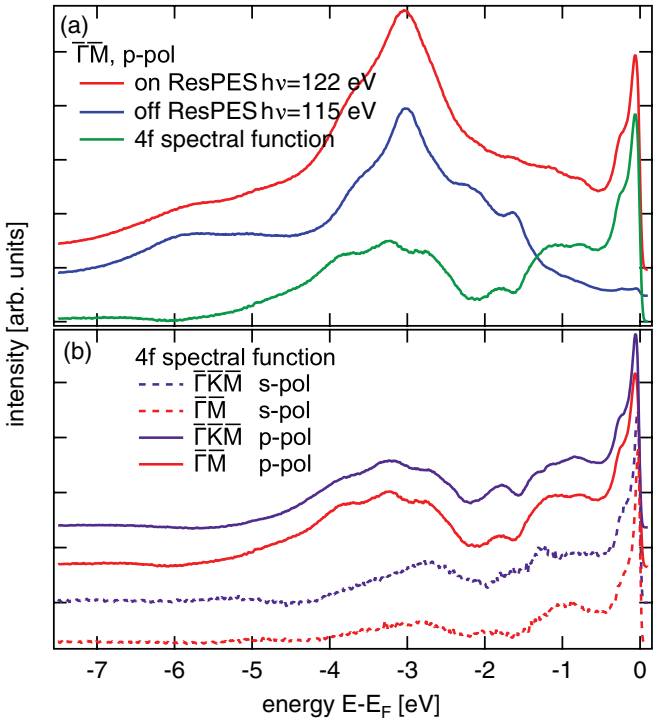

FIG. 3. (Color online) (a) Momentum-integrated spectra for $CePt_5$ measured with p-polarized light along the $\overline{\Gamma M}$ direction off (blue) and on resonance (red) and their difference resembling a measure for the $4f$ spectral function (green). (b) Compilation of $4f$ spectral functions measured along the high-symmetry directions of the surface with s- and p-polarized light.

introduces a step in the hybridization if we assume constant hopping matrix elements between the Ce $4f$ electrons and the conduction states.[17] Considering these findings, the two peaks appearing at $E_B \approx 1$ and 3 eV can be interpreted as a split IS due to a step in the real part of the hybridization in that energy range.

The spectral functions for the other high symmetry directions and light polarizations are displayed in Fig. 3(b). The structures close to the Fermi energy (KR and SO) show a slight dependence on the light polarization: the SO has less spectral weight with respect to the KR with s-polarization. Since the overall spectral weight in the valence band due to the Pt $5d$ electrons is weaker than in the p-polarized spectra we attribute these changes to a polarization dependence of the Pt $5d$ bands. While for this compound, the IS overlaps with the single-particle $5d$ bands of Platinum, it is still possible to remark an important point: The strong Kondo resonance indicates that the Kondo temperature in this sample was higher than in the case of $CeAg_x$ and thus the hybridization between the $4f$ and conduction electrons was stronger. The weaker IS with respect to the Kondo resonance is consistent with the previous conclusions.[17]

C. ARPES band structure

The untypical features in the $4f$ spectral functions can be explained by comparing the ARPES band structure measured with on- and off-resonant photon energies.

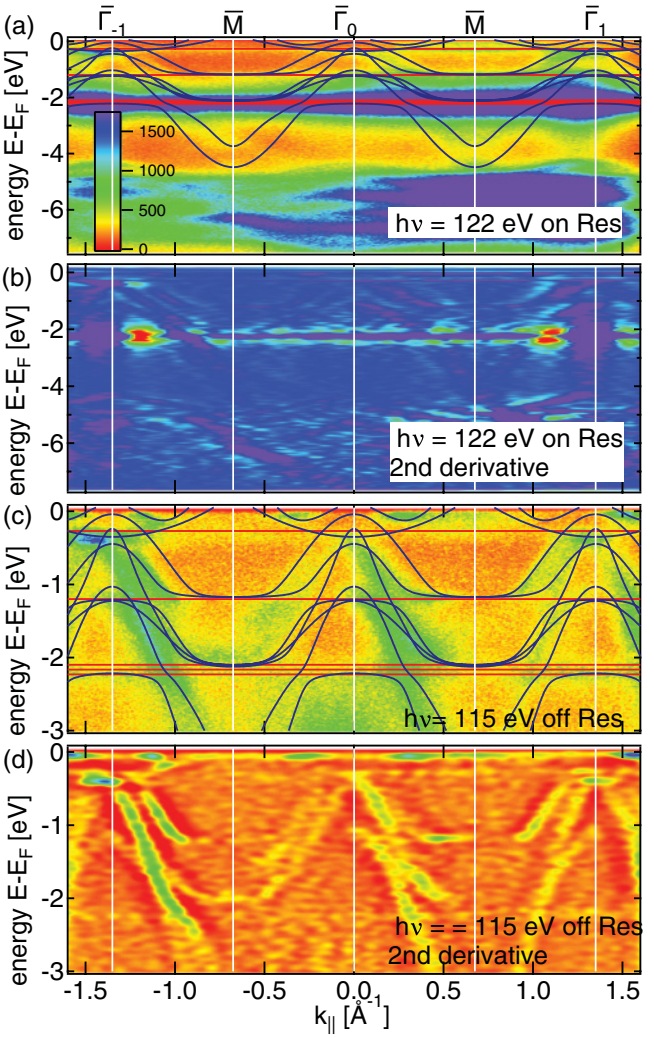

FIG. 4. (Color online) ARPES on $CeAg_x$ surface alloy on the Ag(111) surface along the $\overline{\Gamma M}$ direction with p-polarized light measured with (a) on-resonant photon energy $h\nu = 122$ eV, (b) second derivative thereof, (c) off-resonant photon energy $h\nu = 115$ eV, and (d) second derivative thereof. The off-resonant spectrum and its second derivative only show the region within 3 eV below the Fermi energy. The blue and red lines are guides to the eyes for the dispersing and nondispersing bands, respectively.

1. ARPES band structure of $CeAg_x$/Ag(111)

The on-resonance ARPES spectrum of $CeAg_x$/Ag(111) in Fig. 4(a) shows the Ag $4d$ bands in the energy range 4.5 to 7.5 eV and the IS at $E_B = 2.2$ eV. The much weaker peak at $E_B = 0.27$ eV is the SO partner to the Kondo peak, which shows up as a very small bump at the Fermi energy. The dispersing bands are faint in the on-resonant data and partly masked by the nondispersing cerium states. However, in the off-resonant spectrum in Fig. 4(c) all the bands can be observed having comparable spectral weight.

From the Fermi energy, we find two electron pockets between $|k_{||}| = 0.3$–0.5 Å. Some bands with negative effective mass and a band maximum in the vicinity of the SO partner at the $\overline{\Gamma}$ point are necessary to describe the features at higher binding energy. The shoulder at $E_B = 1.2$ eV in the $4f$ spectral function in Fig. 2(a) can be explained as a flat part of two

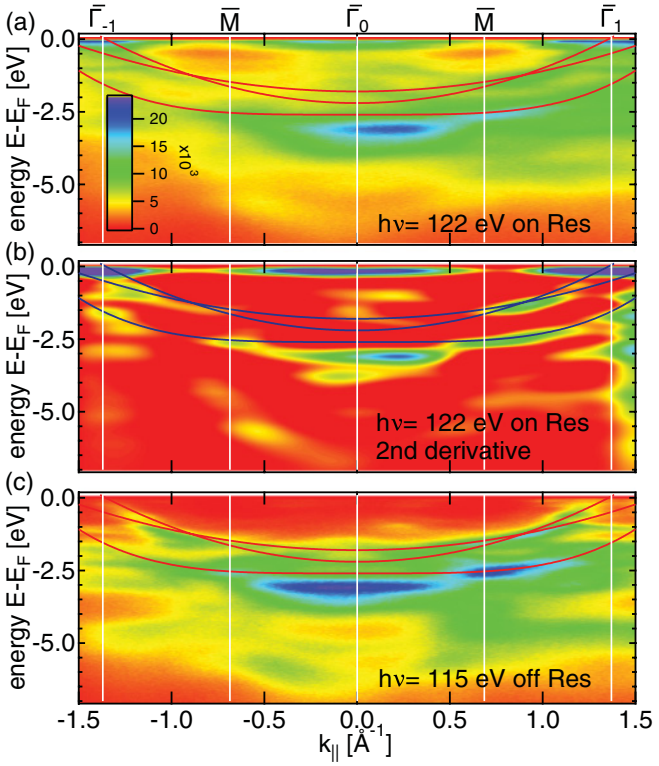

FIG. 5. (Color online) ARPES on $CePt_5$ surface alloy on the Pt(111) surface along the $\bar{\Gamma}\bar{M}$ direction with p-polarized light measured with (a) on-resonant $h\nu = 122$ eV, (c) second derivative thereof, and (b) off-resonant photon energy $h\nu = 115$ eV including red and blue bands as guides for the eyes.

bands in the vicinity of the $\bar{M}$ point. Additionally the IS hybridizes with those lighter bands, resulting in two heavy bands of different binding energies of $E_B = 2.1$ and 2.23 eV, close to the binding energy of the IS in Fig. 2(a).

2. *ARPES band structure of $CePt_5$/Pt(111)*

Figure 5(a) shows the on-resonant ARPES spectrum of $CePt_5$/Pt(111) with the tail of the Kondo resonance right at the Fermi energy, whose intensity is strongly enhanced in the vicinity of the $\bar{\Gamma}$ point. The rest of the on-resonant spectrum is very similar to the off-resonant spectrum, thus attributable to the Pt 5d bands. The electron pockets (marked by guides to the eye in the figure) have their bottom around the $\bar{\Gamma}$ point, but cross the Fermi energy at the $\bar{\Gamma}$ point of the second Brillouin zone. This findings makes us conclude that these bands originate from the substrate: their periodicity is the double of that of the $CePt_5$ alloy, compatible with that of clean Pt(111), which has a twice as large unit cell [see the LEED images of Figs. 1(a) and 1(c)].

3. *Comparison of ARPES band structures of $CeAg_x$ and $CePt_5$*

Comparing the on-resonant ARPES band structure maps in Figs. 4(a) and 5(a) one finds important differences. The binding energies of the Ag 4d bands are in the energy range -4 to -7 eV, while the Pt 5d bands span from the Fermi energy down to a binding energy of 6 eV. Moreover, the actual band dispersion is different for the two alloys, as evidenced by the second derivative of the ARPES data in Figs. 4(b) and 5(b). In $CeAg_x$, all bands (with the exception of the two with the lowest binding energy) have hole character near the $\bar{\Gamma}$ point and positive band mass close to the $\bar{M}$ point. On the other hand, in $CePt_5$ the bands have dominantly positive band mass and show a double periodicity and therefore are assumed to stem from the Pt(111) substrate.

The Ce 4f electrons show different behavior in their nondispersive structures: in $CeAg_x$ most of the 4f signal is in the IS and only a minor contribution comes from the region near the Fermi edge (KR and SO). The opposite is true for $CePt_5$, where the KR is very strong and the IS is so weak that it cannot be resolved from the Pt 5d bands.

V. DISCUSSION

Our findings can be interpreted considering how the hybridization and the Kondo temperature depend on the crystal properties and on the electron filling of silver and platinum. As seen before, the relative strength of the ionization peak with respect to the SO and Kondo peaks may be used to understand the relative weight of the f^0 to f^1 contributions, which mix due to the hybridization term. The strong difference between the spectra presented in Figs. 2 and 3 indicates that the two materials belong to different hybridization regimes, $CeAg_x$ having a much weaker hybridization than $CePt_5$. This implies that the occupation of the f state, n_f, must be very close to 1 for $CeAg_x$ (almost negligible contribution of the f^0 configuration) and sensibly smaller for $CePt_5$, evidence for a stronger contribution of the f^0 configuration. As a consequence the Kondo temperature of $CeAg_x$ has to be much smaller than that of $CePt_5$, $T_{K,CeAg_x} \ll T_{K,CePt_5}$.

In a very simple view, the Kondo temperature should mainly depend on two parameters [see Eq. (1)], namely, the density of conduction band states at E_F and the hybridization between conduction and f states. From the photoemission data both can be estimated roughly but independently. The absolute intensity at the Fermi level in the momentum-integrated off-resonant spectra (Figs. 2 and 3) is proportional to the density of conducting states at the Fermi energy $\rho(E_F)$ times the total photoionization cross section $\sigma(115\text{ eV})$. The latter is twice as large for Pt as for Ag.[24] Whereas at E_F the absolute intensity from $CePt_5$ is 9 times larger than that from $CeAg_x$. Neglecting Ce in the photoemission signal and assuming the same ratio of transition metal atoms per Ce atom (the latter overreaches $CePt_5$) the density of states at the Fermi energy in the two compounds behave as

$$\frac{\rho(E_F)_{CePt_5}}{\rho(E_F)_{CeAg_x}} \approx 5. \qquad (2)$$

The silver 4spd shell is almost completely filled, with binding energies of 4–7 eV, with mainly the 5s and 5p electrons contributing to the conduction in the bulk.[25–27] Even the different structure of $CeAg_x$ with respect to bulk Ag with more inequivalent Ag sites does not increase substantially the density of states at the Fermi energy as can be seen above. On the other hand, the 5d shell of Pt is partially filled, meaning a large density of states at the Fermi energy.[28] Therefore the ratio of density of states already suggests a higher Kondo temperature for $CePt_5$.

Furthermore the hybridization should be immediately correlated to the coordination of the rare-earth atoms; in other words, a larger coordination number should be reflected by a higher Kondo temperature T_K. The crystal structure for $CePt_5$ is well known,[22] and in this $CaCu_5$-type structure the Ce atom is surrounded by 18 Pt atoms.[29] While the structure of the compound $LaAg_5$ has been determined by x-ray diffraction for bulk samples,[30] there is debate on whether a $CeAg_5$ phase even exists in the Ce-Ag phase diagram.[31] Nevertheless an estimation can be pursued for all reported binary phases in the Ce-Ag system. The phase diagram of the Ce-Ag binary alloy shows several candidates where the following number of Ag atoms surround the Ce atom: In $CeAg_1$ 8, in $CeAg_2$ and $CeAg_4$ 12, and in $Ce_{14}Ag_{51}$ the 3 inequivalent cerium atoms are in average surrounded by $15\frac{2}{3}$ silver atoms.[32–34] The interatomic distances can be ignored since they only marginally differ from 1. So for any of the aforementioned Ce-Ag crystal structures, the number of coordination partners of the Ce atom and thus the hybridization are larger in $CePt_5$.

While the higher density of states of $CePt_5$ decreases the (negative) exponent in the Kondo temperature in Eq. (1), this effect is even enhanced by the number of coordination partners. Therefore the Kondo temperatures follow $T_{K,CeAg_x} \ll T_{K,CePt_5}$ in agreement with our experimental results. Moreover the coherent regime, occurring at temperatures $T^* < T_K$, was recently observed experimentally in $CePt_5$ at about 10 K.[1] Thus we conclude that the surface alloy $CeAg_x$ has a vanishing Kondo temperature. In addition these results allow the classification of these systems: $CePt_5$ with its higher hybridization and its higher Kondo temperature has a low f occupancy n_f and thus is more α-like. $CeAg_x$ on the other hand rather belongs to the γ-like Ce compounds because of a weaker hybridization, a lower T_K, and thus a high f occupancy n_f close to 1.[17,21]

VI. CONCLUSION

We reported on the growth and the characterization of the crystal structure of two surface alloys, $CePt_5$ and $CeAg_x$, and on the $4f$ derived spectral features by resonant and angle-resolved photoemission. The two compounds show very different f-spectral functions, whose features are strongly affected by the hybridization parameter of the Anderson model. In turn, the differing hybridizations and consequently the disproportionate Kondo temperatures of the two systems were related to the electron filling of the d shell of the transition metal substrate and to the crystal structure of the surface alloy.

The angle-resolved photoemission data show a complicated underlying electronic structure for both materials with many bands crossing the Fermi energy, a consequence of the presence of several inequivalent atoms in the unit cell. Moreover, it was possible to observe the hybridization between the conduction and the localized bands. In the case of $CePt_5$, the band structure of the Pt substrate was recognized to give a contribution to the ARPES maps thanks to the doubling of the periodicity of the unit cell of the alloy with respect to that of the face-centered cubic Pt(111).

ACKNOWLEDGMENTS

This work was supported by the DFG (Grant No. FOR 1162) and the JSPS (Invitation Program for Advanced Research Institutions in Japan). Synchrotron Radiation Experiments at HiSOR were done under the approval of the HSRC (Proposal No. 10-A-6). Furthermore we thank C. Praetorius, K. Fauth, and F. Assaad for fruitful discussions.

[1] M. Klein, A. Nuber, H. Schwab, C. Albers, N. Tobita, M. Higashiguchi, J. Jiang, S. Fukuda, K. Tanaka, K. Shimada *et al.*, Phys. Rev. Lett. **106**, 186407 (2011).
[2] T. Park, F. Ronning, H. Q. Yuan, M. B. Salamon, R. Movshovich, J. L. Sarrao, and J. D. Thompson, Nature (London) **440**, 65 (2006).
[3] H. Shishido, T. Shibauchi, K. Yasu, T. Kato, H. Kontani, T. Terashima, and Y. Matsuda, Science **327**, 980 (2010).
[4] P. Coleman, Science **327**, 969 (2010).
[5] E. Sagmeister, E. Bauer, E. Gratz, H. Michor, and G. Hilscher, Physica B (Amsterdam) **230–232**, 148 (1997).
[6] A. Schröder, R. van den Berg, H. V. Löhneysen, W. Paul, and H. Lueken, Solid State Commun. **65**, 99 (1988).
[7] R. Takke, N. Dolezal, W. Assmus, and B. Lüthi, J. Magn. Magn. Mater. **23**, 247 (1981).
[8] H. Fujiwara, H. Kadomatsu, and M. Kuriso, J. Magn. Magn. Mater. **31–34**, (Part 1), 189 (1983).
[9] H. Fujiwara, M. Kurisu, and H. Kadomatsu, J. Magn. Magn. Mater. **70**, 369 (1987).
[10] W. J. de Haas, J. H. de Boer, and G. J. van de Berg, Physica **1**, 1115 (1934).
[11] J. Kondo, Prog. Theor. Phys. **32**, 37 (1964).
[12] A. Hewson, *The Kondo Problem to Heavy Fermions* (Cambridge University Press, Cambridge, UK, 1993).
[13] P. W. Anderson, Phys. Rev. **124**, 41 (1961).
[14] S. Hüfner, *Photoelectron Spectroscopy* (Springer-Verlag, Berlin/Heidelberg/New York, 1994).
[15] L. Duò, Surf. Sci. Rep. **32**, 235 (1998).
[16] O. Gunnarsson and K. Schönhammer, *Handbook on the Physics and Chemistry of Rare Earths*, Vol. 10 (North-Holland, Amsterdam, 1987), p. 103.
[17] F. Patthey, J.-M. Imer, W.-D. Schneider, H. Beck, Y. Baer, and B. Delley, Phys. Rev. B **42**, 8864 (1990).
[18] F. Reinert, D. Ehm, S. Schmidt, G. Nicolay, S. Hüfner, J. Kroha, O. Trovarelli, and C. Geibel, Phys. Rev. Lett. **87**, 106401 (2001).
[19] D. Ehm, S. Hüfner, F. Reinert, J. Kroha, P. Wölfle, O. Stockert, C. Geibel, and H. V. Löhneysen, Phys. Rev. B **76**, 045117 (2007).
[20] S. Gardonio, T. O. Wehling, L. Petaccia, S. Lizzit, P. Vilmercati, A. Goldoni, M. Karolak, A. I. Lichtenstein, and C. Carbone, Phys. Rev. Lett. **107**, 026801 (2011).
[21] J. Allen, S. Oh, O. Gunnarsson, K. Schönhammer, M. Maple, M. Torikachvili, and I. Lindau, Adv. Phys. **35**, 275 (1986).
[22] J. M. Essen, C. Becker, and K. Wandelt, J. Surf. Sci. Technol. **7**, 421 (2009).
[23] A. Dal Corso and A. Mosca Conte, Phys. Rev. B **71**, 115106 (2005).
[24] J. Yeh, *Atomic Calculation of Photoionization Cross-Sections and Asymmetry Parameters* (Gordon & Breach, Langhorne, PA, 1993).

[25]G. Panaccione, G. Cautero, M. Cautero, A. Fondacaro, M. Grioni, P. Lacovig, G. Monaco, F. Offi, G. Paolicelli, M. Sacchi *et al*., J. Phys. Condens. Matter **17**, 2671 (2005).
[26]A. Sekiyama, J. Yamaguchi, A. Higashiya, M. Obara, H. Sugiyama, M. Y. Kimura, S. Suga, S. Imada, I. A. Nekrasov, M. Yabashi *et al*., New J. Phys. **12**, 043045 (2010).
[27]Z. Yi, Y. Ma, M. Rohlfing, V. M. Silkin, and E. V. Chulkov, Phys. Rev. B **81**, 125125 (2010).
[28]N. E. Christensen, J. Phys. F **8**, L51 (1978).
[29]K. B. Ameen and M. Bhatia, J. Alloys Compd. **347**, 165 (2002).
[30]O. D. McMasters, K. A. Gschneider Jr., and R. F. Venteicher, Acta Crystallogr. Sec. B **26**, 1224 (1970).
[31]K. Gschneidner and F. Calderwood, J. Phase Equilib. **6**, 439 (1985).
[32]K. Gschneidner and F. Calderwood, J. Phase Equilib. **6**, 439 (1985).
[33]A. C. Larson and D. T. Cromer, Acta Crystallogr. **14**, 73 (1961).
[34]D. M. Bailey and G. R. Kline, Acta Crystallogr. Sec. B **27**, 650 (1971).